Jiang, Y.-J. and Zhao, Y. (2015) ***Géotechnique Letters* 5**, 33–38, http://dx.doi.org/10.1680/geolett.15.00003

Experimental investigation of dry granular flow impact via both normal and tangential force measurements

Y.-J. JIANG* and Y. ZHAO*

The study of granular flow is important for natural hazards such as avalanche and debris flow. In this context, granular flow impact against a retaining wall was investigated through the measurement of both normal and tangential sub-forces. The tangential sub-forces change from positive to negative with respect to the wall in the impact process, which can be classified into two impact states according to the development of the stagnant zone. In the process, interface friction between the granular material and the wall is calculated according to normal and tangential forces and defined as the equivalent interface friction angle, which is observed to vary, and is smaller than the value measured in interface friction tests. The absolute value of the equivalent interface friction angle decreases with slope angle. It was also observed that a reduction in the interface friction angle of the wall has a negligible influence on the impact force calculation, while a reduction in the interface friction angle of the flume base leads to a significant overestimation of the force. These findings should significantly aid the study of granular flow and its applications.

KEYWORDS: earth pressure; laboratory tests; retaining walls; soil/structure interaction

NOTATION

a	empirical constant
C_d	empirical drag coefficient
D_{50}	mean particle diameter (mm)
D_{max}	maximum particle diameter (mm)
D_{min}	minimum particle diameter (mm)
F	total normal force (N/m)
F_{cr}	total normal force at critical time (N/m)
F_d	drag force (N/m)
F_{gf}	gravity- and friction-induced force (N/m)
F_i	normal sub-forces, i = 1–6 (N/m)
F_p	active or passive earth force (N/m)
F_{sum}	total normal force calculated by equation (1) (N/m)
Fr	Froude number
G	weight of stagnant zone (N/m)
$\boldsymbol{g}$	gravitational acceleration (m/s^2)
H	height of initial deposit (m)
h	flow thickness (m)
k_p	passive earth pressure coefficient
L	length of initial deposit (m)
n	empirical constant
T	total tangential force (N/m)
T_{cr}	total tangential forces at critical time (N/m)
T_i	tangential sub-forces, i = 1–6 (N/m)
v	depth-averaged velocity (m/s)
α	slope angle (degrees)
γ_{max}	maximum dry unit weight (kN/m^3)
γ_{min}	minimum dry unit weight (kN/m^3)
δ_1	interface basal friction angle (degrees)
δ_2	interface friction angle of retaining wall (degrees)
δ_3	interface friction angle of side wall (degrees)
δ_{equi}	equivalent interface friction angle (degrees)
θ	angle of repose (degrees)
ρ	density of granular flow (kN/m^3)
ϕ	dynamic internal friction angle (degrees)

Manuscript received 7 January 2015; first decision 28 January 2015; accepted 9 February 2015.
Published online at www.geotechniqueletters.com on 9 March 2015.
*Institute of Mountain Hazards & Environment, Chinese Academy of Sciences, Chengdu, China

INTRODUCTION

Granular flows developed during phenomena such as a landslide or rock avalanche can apply tremendous impact forces on an obstacle in their flow path (Tai *et al.*, 2001; Sovilla *et al.*, 2008; Faug *et al.*, 2011). When a granular flow interacts with a retaining structure such as a retaining wall, a stagnant zone (deposition of granular material) and an inertial layer (flowing layer of granular material) coexist and influence the impact process (Faug *et al.*, 2009; Jiang *et al.*, 2015). Figure 1 illustrates such a case. Depending on the volume of the stagnant zone and the depth of the inertial layer as well as their geometrical relations, the force exerted on a retaining wall can consist of a drag force F_d (Buchholtz & Pöschel, 1998) and an active or passive earth force F_p (Savage & Hutter, 1989), which are generated by the inertial layer, while the stagnant zone can generate a gravity- and friction-induced force (F_{gf}) (Faug *et al.*, 2011; Jiang & Towhata, 2013). In the case that a granular flow is fully trapped by the retaining wall (Fig. 1), the resultant force can be expressed as (Jiang *et al.*, 2015)

$$F = F_d + F_p + F_{gf} = \frac{1}{2}\rho v^2 C_d h + \frac{1}{2}k_p \rho g h^2 \cos\alpha + G\frac{\sin(\alpha-\delta_1)}{\cos(\delta_1+\delta_2)}\cos\delta_2 \quad (1)$$

in which

$$C_d = a\mathrm{Fr}^{-n} = a\left(\frac{v}{(gh)^{1/2}}\right)^{-n}$$

and

$$k_p = \frac{\cos\alpha + (\cos^2\alpha - \cos^2\phi)^{1/2}}{\cos\alpha - (\cos^2\alpha - \cos^2\phi)^{1/2}}$$

In the above equations, C_d denotes the empirical drag coefficient, which is a function of the Froude number (Fr) and two empirical constants, a = 10·8 and n = 1·3 (Thibert *et al.*, 2008), ρ is the density of granular flow, v is the

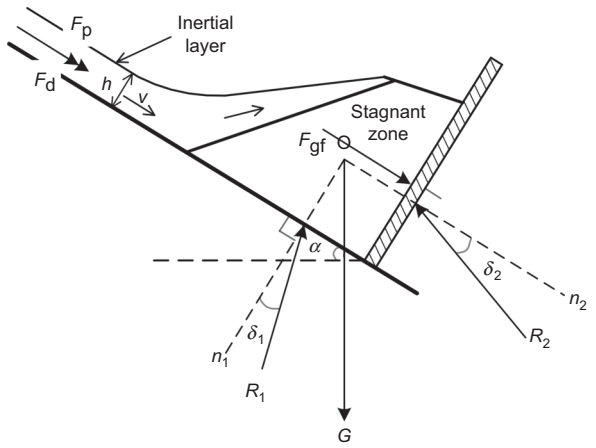

Fig. 1. Schematic illustration of granular flow impact against a retaining wall, in which a part of the granular material is already deposited upstream of the wall to form the stagnant zone, while the layer of flowing granular material continues to impact and flow in the stagnant zone. R_1 and R_2 denote the reaction forces on the flume base and the wall, respectively

depth-averaged velocity, h is the flow thickness, $\boldsymbol{g}$ gravitational acceleration, α the slope angle and ϕ the dynamic internal friction angle. Further, G denotes the weight of the stagnant zone, δ_1 is the interface friction angle of the flume base and δ_2 is the interface friction angle of the retaining wall.

In previous studies (Jiang & Towhata, 2013), only the force normal to the retaining wall surface has been primarily studied, while the influence of the force tangential to the retaining wall has hardly been investigated. This paper thus reports experimental results of granular flow impact studied via measurements of both the normal and tangential forces on a retaining wall. The suitability of equation (1) is also reviewed with a focus on the tangential friction on the retaining wall.

EXPERIMENT

A type of limestone particle, designated particle 1, was selected for this study. Its appearance and particle size distribution are shown in Fig. 2 and typical particle characteristics are listed in Table 1. The interface friction angle was determined by tilting a board until a cylindrical paper container full of granular material placed on the board started to slide (Pudasaini *et al.*, 2007). Instead of direct measurement of the dynamic internal friction angle,

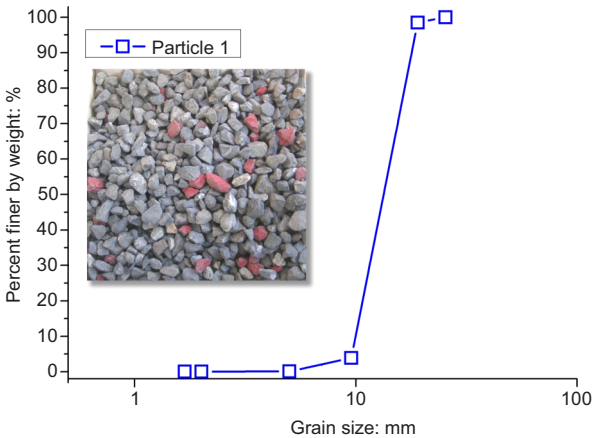

Fig. 2. Particle size distribution of particle 1

Table 1. Physical properties of particle 1

Property	Value
Minimum dry unit weight, γ_{min}: kN/m^3	13·5
Maximum dry unit weight, γ_{max}: kN/m^3	15·4
Mean particle diameter, D_{50}: mm	14·1
Maximum particle diameter, D_{max}: mm	25·4
Minimum particle diameter, D_{min}: mm	1·68
Angle of repose, θ: degrees	47
Dynamic internal friction angle, ϕ: degrees	43
Interface basal friction angle, δ_1: degrees	25
Interface friction angle of retaining wall, δ_2: degrees	21
Interface friction angle of side wall, δ_3: degrees	15

the angle of repose (47°) was first measured by the tilting box method (Burkalow, 1945), which is equal to the static internal friction angle (Miura *et al.*, 1997). It is known the dynamic friction angle is about 4° less than the static internal friction angle (Hungr & Morgenstern, 1984), so the dynamic internal friction angle was determined to be 43°.

An experimental flume with a frictional base was designed to reproduce granular flow in the laboratory, as shown in Fig. 3(a). The experiment considered a granular mass that began flowing from upstream of the flume at a distance of 2·19 m from the wall with an inclination angle of α. Downstream of the flume, two high-speed cameras were positioned to measure the surface velocity and record movement of the granular flow. A retaining wall was divided into six segments and instrumented by six bending-beam load cells. Each of the cells was designed to measure the normal and tangential sub-forces (F_i and T_i, i = 1–6) exerted on the wall, as shown in Fig. 3(b).

The notation used to designate each experiment was based on the length L and height H of the initial deposit and the slope angle α. For instance, particle 1-L44-H20-α45 denotes the experiment using particle 1 with an initial deposit length of 0·44 m, a deposit height of 0·2 m and a slope angle of 45°. The experiments were conducted using different values of L (0·14 m, 0·24 m, 0·34 m and 0·44 m) and H (0·05 m, 0·10 m, 0·15 m and 0·20 m). The slope angle α was also varied (30°, 35°, 40° and 45°). In total, 4 × 4 × 4 = 64 experimental trials were performed.

RESULTS AND DISCUSSION

Normal force and shear force components

For each impact experiment, from the bottom to the top of the wall, the normal and tangential sub-forces (F_1 to F_6 and T_1 to T_6) were measured. The force histories of the experiments designated particle 1-L44-H20-α45 and particle 1-L44-H20-α30 are shown in Figs 4(a) and 4(b), respectively; the upper and lower plots respectively depict the history of the normal and tangential sub-forces. As indicated in Fig. 3, the normal force is referred to as positive when acting towards the face of the retaining wall and the tangential force was assigned as positive when acting in the 'upward' direction of the wall. In both Figs 4(a) and 4(b), it is interesting that, compared with the normal sub-forces, the tangential sub-forces first increase positively and subsequently increase negatively with respect to the retaining wall. Based on the captured motion images, this direction change of the tangential sub-forces can be interpreted as a change in the impact state over time, as shown in Fig. 5. In Fig. 5(a), a thick layer of particles is moving atop a relatively small stagnant zone, directly impacting the retaining wall, and deflecting upward relative to the wall. The upward deflection of the flow layer generates an upward friction on the wall, which explains the positive tangential sub-forces. During the

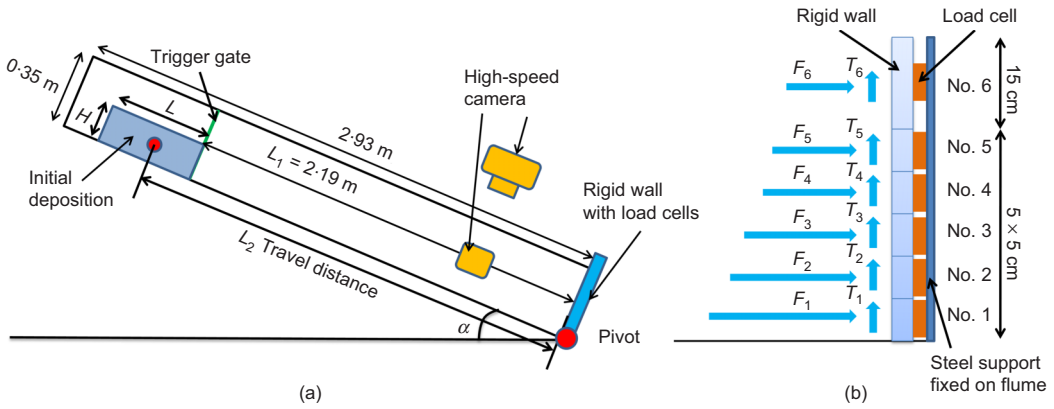

Fig. 3. Experimental flume and retaining wall setup

impact process, more granular material is deposited to form the stagnant zone and, subsequently, the granular flow layer does not directly impact the wall; the friction on the wall is mainly generated by the downward-acting gravity of the stagnant zone, which explains the negative tangential sub-forces.

For analysis purposes, the total normal force F and total tangential force T were first obtained by summing the normal sub-forces and the tangential sub-forces, respectively. A critical time is defined as the time when the maximum F is measured, and the total normal and tangential forces at this instant are defined as F_{cr} and T_{cr}. Figures 6(a) and 6(b) illustrate the history of the F and T values of experiments. From the figures, it is obvious that the critical time for particle 1-L44-H20-α30 is closer to the end of the impact, and its T_{cr} is negative. In contrast, for particle 1-L44-H20-α45, the critical time is closer to the middle of the impact, and both F_{cr} and T_{cr} are positive. The two critical times in Figs 6(a) and 6(b) correspond to the two different impact states shown in Figs 5(a) and 5(b), respectively, and the figures indicate that T_{cr} in the two experiments acts in different directions.

Values of F_{cr} and T_{cr} were deduced for all 64 experiments and thereafter the equivalent interface friction angle (δ_{equi}) was calculated by the arc tangent of T_{cr}/F_{cr}. Since positive and negative values of δ_{equi} respectively indicate the upward and downward directions of the tangential force with respect to the wall, Fig. 7(a) shows the change of direction of tangential force with slope angle. It is clear that the number of δ_{equi} values in the downward direction decreases with an increase in α. This result indicates that, for smaller slope angles, the impact at the critical time tends to the state shown in Fig. 5(b) while, for greater slope angles, the impact state tends to that shown in Fig. 5(a).

The aim of Fig. 7(b) is to show the value of δ_{equi} with no concern for direction; therefore, the absolute value is used. It is interesting that the absolute δ_{equi} is always smaller than the interface friction angle (δ_2) measured by the interface friction test. From Fig. 7(b) it is clear that the maximum absolute value of δ_{equi} is approximately 14° and the minimum is close to 0°: the maximum value is considerably smaller than the measured δ_2 value of 21° (Table 1). In other words, δ_{equi} varies in the impact process and the measured δ_2 cannot be used in equation (1) for force calculation. It is also interesting to observe in Fig. 7(b) that the absolute values of δ_{equi} decrease with increasing α (i.e. δ_{equi} is greater for smaller slope angles).

Influence of interface friction angle on normal force calculation

The above analysis shows that the actual equivalent interface friction angle is smaller than the measured interface friction angle. Therefore, it is necessary to evaluate the effect

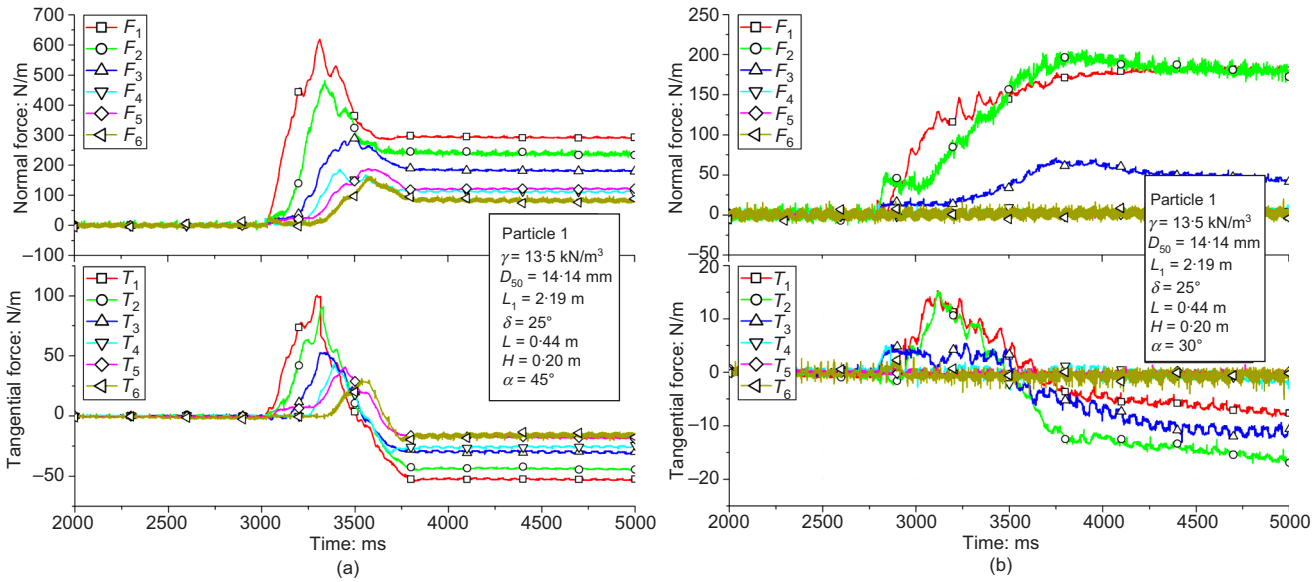

Fig. 4. History of normal and tangential sub-forces: (a) particle 1-L44-H20-α45; (b) particle 1-L44-H20-α30

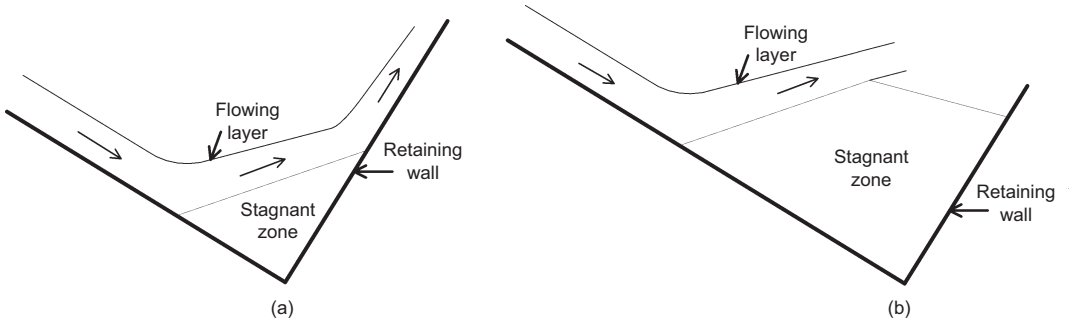

Fig. 5. Two impact states in granular flow impact

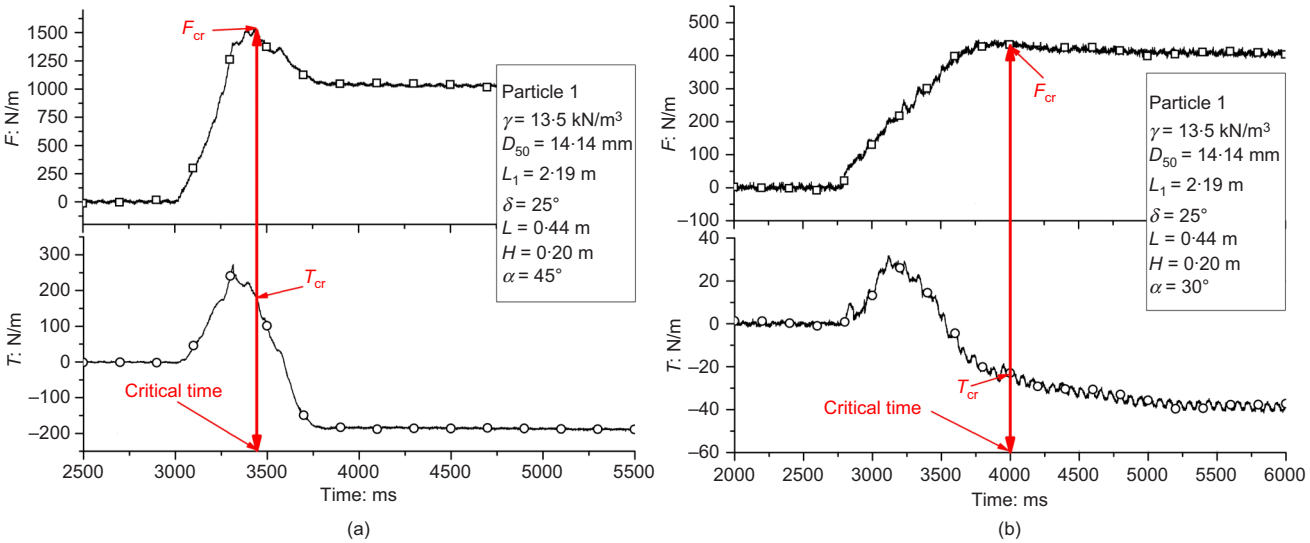

Fig. 6. History of total normal and tangential forces: (a) particle 1-L44-H20-α45; (b) particle 1-L44-H20-α30

of the interface friction angle on the calculation of the normal force using equation (1). First of all, for each experiment, the volume of the stagnant zone, the flow thickness and the velocity at the critical time were measured following the procedure of Jiang *et al.* (2015). Thereafter, the total normal force at the critical time was calculated and designated as F_{sum} by using equation (1) and four different sets of δ_1 and δ_2. As a basis for comparison, $\delta_1 = 25^\circ$ and $\delta_2 = 21^\circ$ were firstly used in equation (1) and the calculated F_{sum} were compared with the measured F_{cr} values, as shown in Fig. 8(a). Figure 8(a) shows that F_{sum} is still quite close to F_{cr}, with a deviation of +30% to −30%, even though we

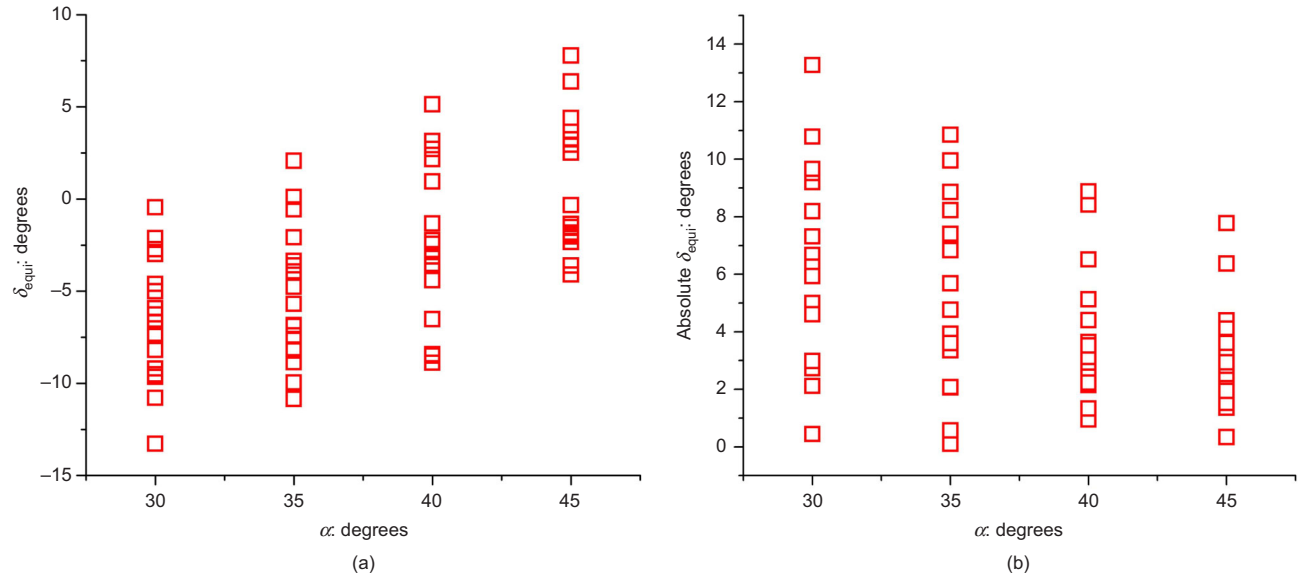

Fig. 7. Variation in δ_{equi} (a) and absolute δ_{equi} (b) with slope angle in the 64 experiments

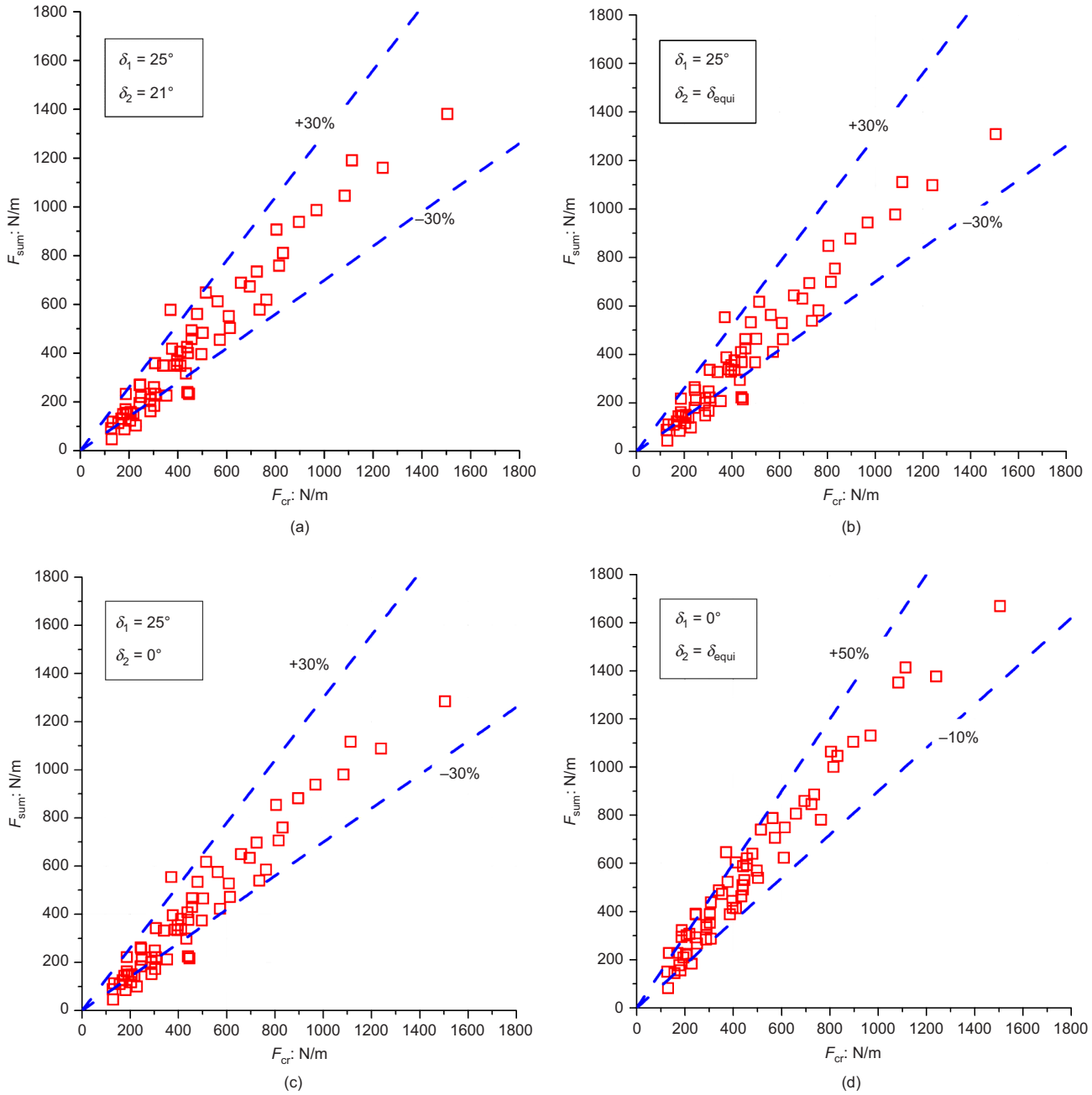

Fig. 8. Influence of interface friction between granular material and wall on total normal force calculation compared with the 64 experimental measurements

know the used δ_2 determined from the interface friction test is overestimated compared with its actual value (δ_{equi}). When $\delta_2 = \delta_{equi}$ (Fig. 8(b)), the result is not significantly different to the case shown in Fig. 8(a). In order to examine the limit of influence of δ_2, δ_2 was set to 0° (Fig. 8(c)); this still had a negligible influence on the calculation of F_{sum}. Thus, reducing δ_2 negligibly influences F_{sum} (Figs 8(a) to 8(c)). Finally, in order to examine the limiting influence of δ_1 on F_{sum}, δ_1 was set to 0°. Figure 8(d) shows that a reduction in δ_1 leads to a significant overestimation of F_{sum}, with a +50% to −10% deviation from the measured F_{cr}.

CONCLUSIONS

The impact of granular flow on a retaining wall was investigated via both normal and tangential sub-force measurements. The following conclusions may be drawn from this study.

- In one granular flow impact process, the tangential sub-forces changed from positive to negative values, which could be interpreted as a transition between two impact states associated with the development of a stagnant zone of material at the base of the retaining wall (Fig. 5).
- In the impact process, the actual equivalent interface friction between the granular material and the wall varies, and is smaller than the value measured in interface friction tests.
- The absolute value of the equivalent interface friction angle (δ_{equi}) decreases with α (i.e. the equivalent friction angle is greater for smaller slope angles).
- For potential designers, an important outcome is that a reduction in the interface friction angle of the retaining wall (δ_2) does not much affect the outcome of F_{sum}, while a reduction in the interface basal friction angle (δ_1)

can produce a significant overestimation of F_{sum}, with a +50% to −10% deviation from the measured F_{cr}.

It is hoped that these findings will contribute to significant developments in granular flow studies.

ACKNOWLEDGEMENTS

The authors express their sincere gratitude for support from the National Natural Science Foundation of China (grant 41030742) and the Hundred Young Talents Program of the Institute of Mountain Hazards and Environment (grant SDSQB-2013–01). The support of the West Light Foundation of Chinese Academy of Sciences and the Science Foundation of the Institute of Mountain Hazards and Environment for Young Scholars is also gratefully acknowledged.

REFERENCES

Buchholtz, V. & Pöschel, T. (1998). Interaction of a granular stream with an obstacle. *Granul. Matter* **1**, No. 33, 33–41.

Burkalow, A. (1945). Angle of repose and angle of sliding friction: an experimental study. *Geol. Soc. Am. Bull.* **56**, No. 6, 669–707.

Faug, T., Beguin, R. & Chanut, B. (2009). Mean steady granular force on a wall overflowed by free-surface gravity-driven dense flows. *Phys. Rev. E* **80**, No. 2, Part 1, 021305.

Faug, T., Caccamo, P. & Chanut, B. (2011). Equation for the force experienced by a wall overflowed by a granular avalanche: experimental verification. *Phys. Rev. E* **84**, No. 5, Part 1, 051301.

Hungr, O. & Morgenstern, N. R. (1984). Experiments on the flow behavior of granular materials at high velocity in an open channel flow. *Géotechnique* **34**, No. 3, 405–413.

Jiang, Y.-J. & Towhata, I. (2013). Experimental study of dry granular flow and impact behavior against a rigid retaining wall. *Rock Mech. Rock Engng* **46**, No. 4, 713–729.

Jiang, Y.-J., Zhao, Y., Towhata, I. & Liu, D.-X. (2015). Influence of particle characteristics on impact event of dry granular flow. *Powder Technol.* **270**, Part A, 53–67.

Miura, K., Maeda, K. & Toki, S. (1997). Method of measurement for the angle of repose of sands. *Soils and Found.* **37**, No. 2, 89–96.

Pudasaini, S. P., Hutter, K., Hsiau, S.-S., Tai, S.-C., Wang, Y. & Katzenbach, R. (2007). Rapid flow of dry granular materials down inclined chutes impinging on rigid walls. *Phys. Fluids* **19**, No. 5, 053302.

Savage, S. B. & Hutter, K. (1989). The motion of a finite mass of granular material down a rough incline. *J. Fluid Mech.* **199**, 177–215.

Sovilla, B., Schaer, M., Kern, M. & Bartelt, P. (2008). Impact pressures and flow regimes in dense snow avalanches observed at the Vallée de la Sionne test site. *J. Geophys. Res.* **113**, No. 1, F01010.

Tai, Y. C., Gray, J. M. N. T., Hutter, K. & Noelle, S. (2001). Flow of dense avalanches past obstructions. *Ann. Glaciol.* **32**, No. 1, 281–284.

Thibert, E., Baroudi, D., Limam, A. & Berthet-Rambaud, P. (2008). Avalanche impact pressure on an instrumented structure. *Cold Reg. Sci. Technol.* **54**, No. 3, 206–215.